

Finite difference numerical method for the superlattice Boltzmann transport equation and case comparison of CPU(C) and GPU(CUDA) implementations

Dmitri Priimak

Department of Physics, Loughborough University LE11 3TU, United Kingdom

Abstract

We present a finite difference numerical algorithm for solving two dimensional spatially homogeneous Boltzmann transport equation which describes electron transport in a semiconductor superlattice subject to crossed time dependent electric and constant magnetic fields. The algorithm is implemented both in C language targeted to CPU and in CUDA C language targeted to commodity NVidia GPU. We compare performances and merits of one implementation versus another and discuss various software optimization techniques.

Keywords: Boltzmann equation; Superlattice; Finite Difference Method; GPU; CUDA

1. Introduction

Numerical solutions of Boltzmann Transport Equation (BTE) are of utmost importance in the modern physics, especially in the research areas of fluid dynamics and semi-classical description of quantum-mechanical systems. BTE is often solved using Monte-Carlo method [1]. The other approach is Lattice Boltzmann Method, it is more recent and very promising [2]. Due to its numerical stability and explicit nature, Lattice Boltzmann Method lends itself quite well to the parallel implementations on Graphical Processing Units (GPU) [3, 4, 5, 6]. Finite Difference Method (FDM) is the simplest approach to the solution of BTE. However, to attain desirable numerical stability it often requires fully implicit formulation. Recently, a number of new advanced FDMs were developed. In [7] a variant of FDM is combined with Monte-Carlo method. Fully functional solver for PMOSFET devices, which among other things can utilize FDM for solving BTE, was presented in [8]. Numerical method for spatially non-homogeneous 1D BTE in application to semiconductor superlattices was recently considered in [9].

In this work, we present a FDM method for solving two-dimensional BTE that describes a semiconductor superlattice (SL) subject to a time dependant electric field along the superlattice axis and a constant perpendicular magnetic field. SL and the configuration of applied fields are sketched in Fig.1. This problem was earlier considered only in the limiting case of zero temperature [10], while our numerical scheme and software that implements it, are used to analyse electron dynamics in SL at arbitrary temperatures. Superlattices are artificial periodic structures with periods not found in natural solids [12]. This relatively large period of SL results in a number of its unique physical features, which are interesting not only from the viewpoint of fundamental properties of solids, but also as tools in a realization of promising applications, including the generation and detection of terahertz radiation. Good overview of SL theory and basic experiments can be found in [11].

Our numerical method combines Crank-Nicolson [13] and leap-frog algorithms. Leap-frog algorithm is a variant of symplectic integrators, which are known to preserve area in the phase space and are unconditionally stable [14, 15]. We develop several implementations of our algorithm. One implementation uses C programming language and is targeted for CPU. Other implementations are written in CUDA and are targeted at NVidia GPU. Compute Unified Device Architecture, also known as CUDA, is parallel computing

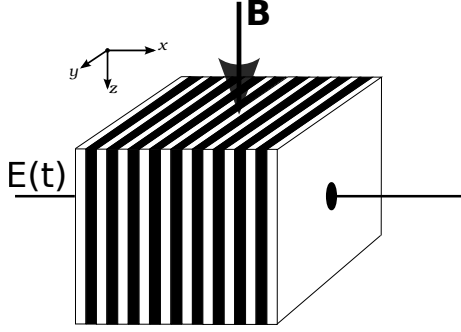


Figure 1: Sketch of a superlattice under the action of time dependent electric $E(t)$ and constant magnetic \mathbf{B} fields. The electric field is directed along the superlattice axis (x -axis) and the perpendicular magnetic field is aligned along z -axis. Electron motion is considered in (x, y) -plane.

platform and C/C++ language extension for NVidia video cards. Different CUDA implementations of our numerical method primarily highlights various differences in memory access patterns, which are the most common bottlenecks for software running on video cards. We verified correctness of the method and its implementation by comparing our results of simulations with the available analytical results in the limiting case of zero temperature.

2. Physical model

Boltzmann equation governs a time evolution of the electron probability density function $f(t, \mathbf{k}, \mathbf{r})$. For our system it has the following form

$$\frac{\partial f}{\partial t} + \frac{e}{\hbar} (\mathbf{E} + \mathbf{v} \times \mathbf{B}) \frac{\partial f}{\partial \mathbf{k}} + \mathbf{v}(\mathbf{k}) \frac{\partial f}{\partial \mathbf{r}} = \left(\frac{\partial f}{\partial t} \right)_{st} \quad (1)$$

$$\mathbf{v}(\mathbf{k}) = \frac{1}{\hbar} \frac{\partial \varepsilon}{\partial \mathbf{k}} \quad (2)$$

where \mathbf{k} is the crystal momentum, $\mathbf{v}(\mathbf{k})$ is the electron velocity and $\varepsilon(\mathbf{k})$ is the energy dispersion relation for the lowest SL miniband [11]. We make several simplifications. Firstly, we assume that f is spatially homogeneous and put $\partial f / \partial \mathbf{r} = 0$. Secondly, the collision integral $(\partial f / \partial t)_{st}$ is taken in the most simplest form $(f_0 - f) / \tau$, where f_0 is the equilibrium distribution function and τ is the constant relaxation time. We also limited our consideration to electron transport in a single miniband, which we describe within a tight binding approximation

$$\varepsilon = \frac{\hbar^2 k_y^2}{2m} - \frac{\Delta_1}{2} \cos(k_x d) \quad (3)$$

where Δ is the width of the miniband and m is the effective electron mass along SL layers. To make this system of equations (1) (2) and (3) dimensionless we make following substitutions.

$$\begin{aligned} \phi_x &= k_x d & \phi_y &= k_y d / \sqrt{\alpha} \\ E/E_* &\rightarrow E & E_* &= \frac{\hbar}{ed\tau} \\ eB\tau/\sqrt{mm_x} &\rightarrow B & t &\rightarrow t\tau \\ \alpha &= m/m_x & m_x &= \frac{2\hbar^2}{\Delta_1 d^2} \end{aligned} \quad (4)$$

And in view of geometry of our system (Fig. 1) we obtain the following form of Boltzmann equation in dimensionless variables

$$\frac{\partial f}{\partial t} + (E + B\phi_y) \frac{\partial f}{\partial \phi_x} - B \sin(\phi_x) \frac{\partial f}{\partial \phi_y} = f_0 - f \quad (5)$$

The probability density function $f(t, \phi_x, \phi_y)$ can formally extend indefinitely along the y -axis, but practically this extension is always effectively limited by a relaxation to the equilibrium distribution $f_0(\phi_x, \phi_y)$. In SL $f(t, \phi_x, \phi_y)$ is periodic along the x -axis with the period 2π . Therefore, ϕ_x can be considered only within the first Brillouin zone defined from $-\pi$ to π . The periodicity allows us to represent both f and f_0 in the form of Fourier series

$$f_0 = \sum_{n=0}^{\infty} a_n^{(0)} \cos(n\phi_x) \quad (6)$$

$$f = \sum_{n=0}^{\infty} a_n \cos(n\phi_x) + b_n \sin(n\phi_x) \quad (7)$$

where the Fourier coefficients $a_n^{(0)}$, a_n and b_n are functions of ϕ_y and the last two are also functions of time. In the Fourier representation, Boltzmann equation (5) takes the form of an infinite set of the ordinary differential equations

$$\frac{\partial a_n}{\partial t} = a_n^{(0)} - a_n - n(E + B\phi_y)b_n + \frac{B}{2} \left(\frac{\partial b_{n+1}}{\partial \phi_y} - \frac{\partial b_{n-1}}{\partial \phi_y} \right) \quad (8)$$

$$\frac{\partial b_n}{\partial t} = -b_n + n(E + B\phi_y)a_n + \frac{B}{2} \left(\chi(n) \frac{\partial a_{n-1}}{\partial \phi_y} - \frac{\partial a_{n+1}}{\partial \phi_y} \right) \quad (9)$$

$$(10)$$

$$\chi(n) = \begin{cases} 2 & : n = 1 \\ 1 & : n \neq 1 \end{cases} \quad (11)$$

The equilibrium probability density function is assumed to be a temperature-dependent Boltzmann distribution, which with all normalization constants takes the form

$$f_0 = \frac{1}{2\pi I_0(\mu)} \sqrt{\frac{\mu}{2\pi\alpha}} \exp \left\{ \mu \cos(\phi_x) - \frac{\mu}{2} \phi_y^2 \right\} \quad (12)$$

$$\mu = \frac{\Delta_1}{2k_b T} \quad (13)$$

Where $I_0(\mu)$ is modified Bessel function of zeroes order. We can use this specific form of f_0 to find Fourier coefficients $a_n^{(0)}$

$$a_n^{(0)} = \frac{\sigma(n) I_n(\mu)}{\pi I_0(\mu)} \sqrt{\frac{\mu}{2\pi\alpha}} \exp \left\{ -\frac{\mu}{2} \phi_y^2 \right\} \quad (14)$$

$$\sigma(n) = \begin{cases} 1/2 & : n = 0 \\ 1 & : n \neq 1 \end{cases} \quad (15)$$

where $I_n(\mu)$ are the modified Bessel functions of order n . Equations (8) and (9) do not preclude time dependency of both the electric E and magnetic B fields. However, keeping in line with the existing research in this field [10], here we consider a constant B and the electric field that is a sum of a constant E_{dc} and monochromatic ac $E_\omega \cos(\omega t)$ components. Thus the total electric field acting on electrons in SL is $E = E_{dc} + E_\omega \cos(\omega t)$. We were most interested in property of absorption of ac component of electric field. When negative it indicates ac field amplification, paving the way to a lasing medium. We define absorption as a following expression time averaged over period $2\pi/\omega$.

$$A = \left\langle \frac{2I_0(\mu)v_{dr}}{I_1(\mu)} \cos(\omega t) \right\rangle_t \quad (16)$$

where v_{dr} is electron drift velocity along the x -axis.

$$v_{dr} = \frac{2d}{\Delta_1 \hbar} \iint \frac{\partial \varepsilon}{\partial p_x} f(p_x, p_y) dp_x dp_y \quad (17)$$

$$= \sqrt{\alpha} \int_{-\pi}^{\pi} d\phi_x \int_{-\infty}^{+\infty} d\phi_y \sin(\phi_x) f(\phi_x, \phi_y) \quad (18)$$

which in view of Fourier expansion of f (7) takes form

$$v_{dr} = \pi \sqrt{\alpha} \int_{-\infty}^{+\infty} b_1(\phi_y) d\phi_y \quad (19)$$

Independently of numerical method, norm of electron density function f has to always be equals to one, which in our coordinates takes form

$$\sqrt{\alpha} \int_{-\pi}^{\pi} d\phi_x \int_{-\infty}^{+\infty} d\phi_y f(\phi_x, \phi_y) = 1 \quad (20)$$

$$2\pi \sqrt{\alpha} \int_{-\infty}^{+\infty} a_0(\phi_y) d\phi_y = 1 \quad (21)$$

Eq. (21) is later used as one of the tests of accuracy of our numerical method.

3. Numerical algorithm

Naive application of method of finite difference to (8) and (9) leads to either unstable and/or computationally intensive numerical system. To combat this problem we are using several methods at once. First, we discretize a_n and b_n along time and ϕ_y axes.

$$\begin{aligned} t &\leftarrow \text{time step} \\ a_{n,m} &\leftarrow \phi_y \text{ lattice step} \end{aligned} \quad (22)$$

and n is "harmonic number". This forms infinite two-dimensional grid. To be computable we limit it to $n \in [0, \dots, N]$ and $m \in [0, \dots, M]$, with following boundary conditions.

$$a_{n \notin [0, \dots, N], m \notin [0, \dots, M]} = 0 \quad (23)$$

$$b_{n \notin [1, \dots, N], m \notin [0, \dots, M]} = 0 \quad (24)$$

Both upper limits N and M have to be adjusted manually depending on strength of electric and magnetic fields and inverse temperature μ , which smears distribution function f in the phase space. Along the y -axis ϕ_y is discretized with step $\Delta\phi$ and it becomes function of lattice number m .

We write two forms of equations (8) and (9). One using forward differences and one using partial backward differences, i.e. on the right side of equal sign we are going to write partial derivatives at time t while everything else at time $t + 1$ and will follow standard procedure of Crank-Nicolson scheme by adding these two, forward and backward differences equations. First two equations (25) and (26) below are written

in forward differencing scheme and last two (27) and (28) in backward differencing scheme

$$a_{n,m}^{t+1} - a_{n,m}^t = a_{n,m}^{(0)} \Delta t - a_{n,m}^t \Delta t - 2b_{n,m}^t \mu_{n,m}^t + \frac{\alpha B \Delta t}{4\Delta\phi} (b_{n+1,m+1}^t - b_{n+1,m-1}^t - b_{n-1,m+1}^t + b_{n-1,m-1}^t) \quad (25)$$

$$b_{n,m}^{t+1} - b_{n,m}^t = -b_{n,m}^t \Delta t + 2a_{n,m}^t \mu_{n,m}^t + \frac{\alpha B \Delta t}{4\Delta\phi} (\chi(n)[a_{n-1,m+1}^t - a_{n-1,m-1}^t] - a_{n+1,m+1}^t + a_{n+1,m-1}^t) \quad (26)$$

$$a_{n,m}^{t+1} - a_{n,m}^t = a_{n,m}^{(0)} \Delta t - a_{n,m}^{t+1} \Delta t - 2b_{n,m}^{t+1} \mu_{n,m}^{t+1} + \frac{\alpha B \Delta t}{4\Delta\phi} (b_{n+1,m+1}^t - b_{n+1,m-1}^t - b_{n-1,m+1}^t + b_{n-1,m-1}^t) \quad (27)$$

$$b_{n,m}^{t+1} - b_{n,m}^t = -b_{n,m}^{t+1} \Delta t + 2a_{n,m}^{t+1} \mu_{n,m}^{t+1} + \frac{\alpha B \Delta t}{4\Delta\phi} (\chi(n)[a_{n-1,m+1}^t - a_{n-1,m-1}^t] - a_{n+1,m+1}^t + a_{n+1,m-1}^t) \quad (28)$$

where

$$\beta_m^t = E^t + B^t \phi_y(m) \quad (29)$$

$$\mu_{n,m}^t = n \beta_m^t \Delta t / 2 \quad (30)$$

And application of Crank-Nicolson scheme [13] leads to

$$a_{n,m}^{t+1} = \frac{g_{n,m}^t \nu - h_{n,m}^t \mu_{n,m}^{t+1}}{\nu^2 + (\mu_{n,m}^{t+1})^2} \quad (31)$$

$$b_{n,m}^{t+1} = \frac{g_{n,m}^t \mu_{n,m}^{t+1} - h_{n,m}^t \nu}{\nu^2 + (\mu_{n,m}^{t+1})^2} \quad (32)$$

where

$$\nu = 1 + \Delta t / 2 \quad (33)$$

$$\xi = 1 - \Delta t / 2 \quad (34)$$

$$g_{n,m}^t = a_{n,m}^t \xi - b_{n,m}^t \mu_{n,m}^t + B_{n,m}^t + a_{n,m}^{(0)} \Delta t \quad (35)$$

$$h_{n,m}^t = b_{n,m}^t \xi + a_{n,m}^t \mu_{n,m}^t + A_{n,m}^t \quad (36)$$

$$A_{n,m}^t = \frac{\alpha B \Delta t}{4\Delta\phi} (\chi(n)[a_{n-1,m+1}^t - a_{n-1,m-1}^t] - a_{n+1,m+1}^t + a_{n+1,m-1}^t) \quad (37)$$

$$B_{n,m}^t = \frac{\alpha B \Delta t}{4\Delta\phi} (b_{n+1,m+1}^t - b_{n+1,m-1}^t - b_{n-1,m+1}^t + b_{n-1,m-1}^t) \quad (38)$$

Equation (31, 32) can be formally written in the form

$$\mathbf{z}_{n,m}^{t+1} = \mathbf{T}(\mathbf{z}_{n,m}^t; A_{n,m}^t, B_{n,m}^t) \quad (39)$$

$$\mathbf{z}_{n,m}^t = (a_{n,m}^t, b_{n,m}^t) \quad (40)$$

Where \mathbf{T} is an operator that allows us to step from time step t to $t+1$, separated by time interval Δt . Using this operation as is leads to only conditionally stable numerical system, because $A_{n,m}^t$ and $B_{n,m}^t$ are taken at time t , i.e. partially this is still simple forward difference scheme. To combat this problem we introduce two staggered grids $\{\mathbf{z}^0, \mathbf{z}^1, \dots\}$ and $\{\mathbf{z}^{1/2}, \mathbf{z}^{3/2}, \dots\}$, which we call *whole* and *fractional* one respectively. We then

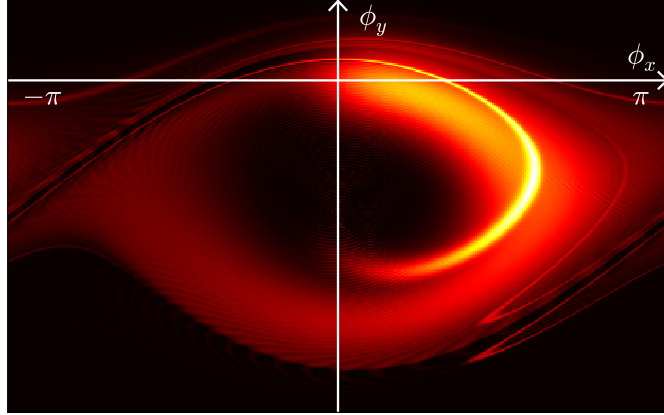


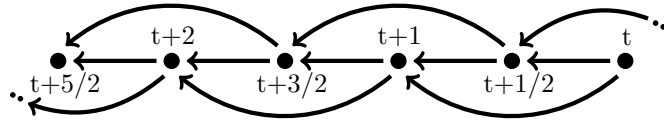
Figure 2: Example of result of numerical simulation showing transient response of electron probability density function (PDF) in the phase space (ϕ_x, ϕ_y) in response to applied electric and magnetic fields. Here electric field is applied along the ϕ_x axis and magnetic field perpendicular to the plane of the plot. Initially PDF is concentrated around center of the plot according to Boltzmann distribution function (12).

use leap frog method where to calculate \mathbf{z}^{t+1} using (39) we use $A^{t+1/2}$ and $B^{t+1/2}$ computed on fractional grid. Similar operation is performed for a step from $t+1/2$ to $t+3/2$. Thus one step from t to $t+1$ becomes two steps.

$$\mathbf{z}_{n,m}^{t+1} = \mathbf{T}(\mathbf{z}_{n,m}^t; A_{n,m}^{t+1/2}, B_{n,m}^{t+1/2}) \quad (41)$$

$$\mathbf{z}_{n,m}^{t+3/2} = \mathbf{T}(\mathbf{z}_{n,m}^{t+1/2}; A_{n,m}^{t+1}, B_{n,m}^{t+1}) \quad (42)$$

And steps alternate as seen in the following picture



This algorithm has to be started first by computing values of $\mathbf{z}^{1/2}$ using (39) with time step $\Delta t/2$. In Fig.2 you can see example of computing of probability density function using our algorithm. This figure shows heat-map plot of transient response of the system to applied electric and magnetic fields according to geometry as shown in Fig. 1.

4. CUDA and GPU computing overview

Modern GPU differ from CPU in that they have thousands ALUs¹ at the expense of control hardware and large implicit caches of CPUs. In NVidia video cards these ALUs are known as "CUDA cores". They are grouped into rows and rows into larger units with control hardware and explicit caches. These units are known as Streaming Multiprocessors (SMX). In turn a single card often contains dozen of SMX units. Abundance of ALUs makes for a need of dedicated memory and wide memory bus directly on GPU. For example in GTX680 memory bandwidth is approximately 192GB/sec., while Intel Core i7 CPU with sandy bridge architecture provides only 37GB/sec of aggregate bandwidth. In general all of the ALUs in a video card can be executed in parallel, although in actuality their execution in SMXs is scheduled in groups of 32 threads known as warps. This very large degree of parallelism commonly leads to saturation of memory

¹Arithmetic Logic Unit

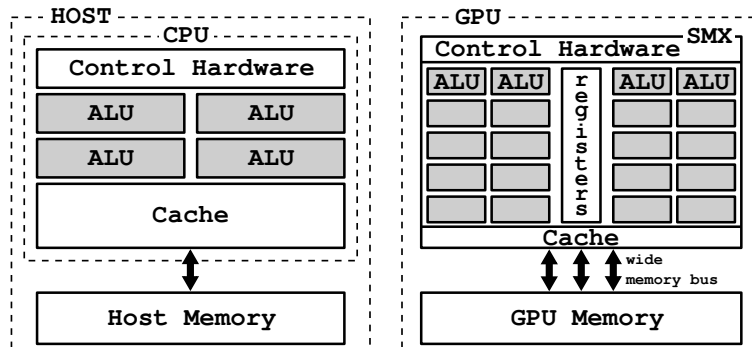


Figure 3: Simplified logical scheme of host computer and GPU that highlights differences between two. Notable is abundance of ALUs in modern day GPU, which reaches into thousands and fast wide memory bus comparing to slow memory bus on the host computer.

bus between on-board GPU memory and SMXs, which means that while programming for GPU significant speed enhancements can be made by optimising memory access patterns and using explicitly available caches [4, 16, 17]. Misaligned and uncoalesced memory access is much slower than indicated by maximum available bandwidth. Such access patterns are common problem points in CUDA programs. Thus in general CUDA software should try to minimize writing and reading to and from memory. It is common to refer to main computer as *host* and installed GPU as *device*. Simplified logical layout of host and GPU can be seen in Fig. 3. Generally speaking GPU can be thought of as an explicitly programmable co-processor. White paper describing latest Kepler architecture of NVidia GPU can be found in [18].

CUDA is general purpose computing environment and extension to C and C++ languages developed by NVidia. It extends physical abstractions of GPU briefly described above and presents coherent API² for developing general purpose software [19]. Basic introduction to CUDA programming can be found in [20] and much more comprehensive one in [21]. Software written for a GPU always consist of two parts. One part that runs on the host computer, aka host code, and another part that runs on the device, aka kernel code. It is very common in one program to have several kernels executing in sequence or in parallel, later one is possible with CUDA streams. Kernels are implicitly loaded onto the device by CUDA runtime. They can access data structures stored on both, on-board device memory and much slower, but usually much larger host memory. To be placed on the on-board device memory, data structures have to be created first on the host computer and then explicitly loaded onto the device (GPU). Execution of a kernel happens in parallel up to the capacity of the device to do so. Each parallel flow of execution is known as a *thread*. Threads are organized in hierarchy of grid of blocks of threads. Threads within a block can share information through very fast shared memory. Significant amount of even faster register memory also available for each thread. Number of blocks and number of threads per block have upper limits. For GTX680 GPU grids containing blocks can be three-dimensional with maximum number of blocks $65535 \times 65535 \times 65535$ and number of threads per blocks is limited to 1024 giving total number of threads an astonishing value of 2^{58} . We can think of all of them as executing in parallel although in reality parallelism is ultimately limited by total number of available ALUs. At the simplest level CUDA programming could be understood as converting inner content of a loop into kernel code and replacing it with invocation of a kernel on the device. Inside of a kernel, index variable provided by a loop is replaced by a set of implicit variables indicating block number and thread number within a block. Together with dimensions of a block and grid they can be used to compute an equivalent of loop index. This is illustrated in the code snippet below, where only one of implicit variables `threadIdx` is shown. It defines position of thread within a block.

²Application Programming Interface

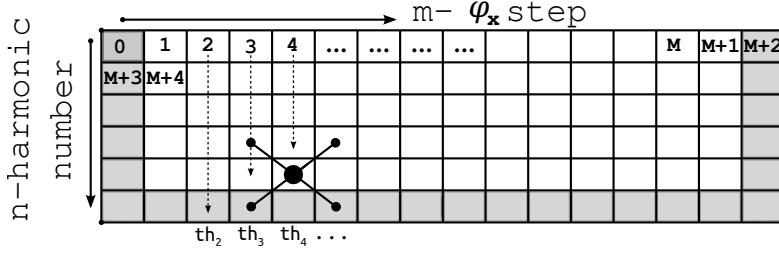


Figure 4: Raw-major layout of $a_{n,m}$ and $b_{n,m}$ arrays in linear memory. Grayed out blocks correspond to boundary conditions. They have constant values of 0 and are not modified. This allows to avoid diverging data flows among groups of threads. One thread is spawned for each m number, shown with dashed line. Each thread, shown as th_1, th_2 etc., is responsible for computing next values of a and b arrays across all n harmonic numbers. Cross pattern within array shows neighbouring points that are needed to compute next value of point in the center (shown with large black circle).

```

for i in [0,...,N]      compute_kernel()
    compute(i)          →   i := threadIdx.x
end                    ...
                        end

```

This kernel is later called with parameters indicating number of threads per block and number of blocks.

5. C and CUDA implementations

Using above mentioned algorithm two software packages were written. The C version that targets CPU and C/CUDA version for running on NVidia GPU. CUDA version was tested on consumer grade video card GTX680. Both implementations share the same memory layout. For C implementation memory layout is not important because computation is limited by speed of CPU. For CUDA version computation is limited by I/O speed between memory in a GPU and total number of available ALUs. Thus layout of arrays storing $a_{n,m}^{(0)}$, $a_{n,m}$ and $b_{n,m}$ and memory access patterns makes for the biggest difference in performance. We used a raw-major layout shown in Fig. 4. To avoid divergent data flow at the boundaries we shift m index to the right and introduce zero cells along the perimeter of each array. These zero cells, highlighted in gray in Fig. 4, ensure that boundary conditions (23) (24) are satisfied without use of `if` statements. Each thread computes next values of a and b for all of harmonic numbers for a given m value. In total we define 9 two-dimensional arrays. $a_{n,m}^{(0)}$ as `a0(n,m)`. On the whole grid $a_{n,m}$ as `a.h([0,1],n,m)` and $b_{n,m}$ as `b.h([0,1],n,m)` and on the fractional one `a.f([0,1],n,m)` and `b.f([0,1],n,m)`. First index in `a` and `b` arrays can take only values of 0 or 1 and is used to alternate between current t and next $t+1$ steps. Both CPU and GPU implementations share this logic and a time loop, which is shown below. This time loop is a part of a host code.

```

Time loop
-----
cur, nxt := 0, 1
for t in [0, ..., T_max]
    compute_time_step(t, cur, nxt)
    cur, nxt := nxt, cur
end
-----

```

Where `compute_time_step(...)` function performs movement in time from t and $t+1/2$ to $t+1$ and $t+3/2$ respectively. Implementation targeted to CPU implements this function as shown in the following snippet.

CPU implementation

```

for m in [1,...,M+1]
  for n in [0,...,N]
    a_h(nxt, n, m) :=
      T(a_h(cur,n,m), a_f(cur,n-1,m-1), a_f(cur,n-1,m+1),
        a_f(cur, n+1, m-1), a_f(cur, n+1, m+1))
    b_h(nxt, n, m) := ...
  end
end
end

```

where $T(\dots)$ is implementation of operator (39). These code is repeated once more to compute a and b on fractional grid. There are several ways this can be transformed into a CUDA code. Two kernels are formed. One to move forward in time on the whole grid and another one for the fractional grid. Within each of the kernels several variants are possible. We identify each kernel as K_x , where x is implementation number. The simplest one (K_1) is where one thread is allocated for each point of the grid. In K_2 (not shown below) we load a and b into `__shared__` array, which is first level of explicit cache in NVidia GPU.

| K_1 | K_3 |
|--|--|
| <pre> kernel_1(...) m := ... n := ... a_h(nxt, n, m) := ... b_h(nxt, n, m) := ... end </pre> | <pre> kernel_3(...) m := ... for n in [0,...,N] a_h(nxt, n, m) := ... b_h(nxt, n, m) := ... end end </pre> |

This way we can reduce memory access since nearby threads do access the same data structures. However, they share very little data and while benefits are noticeable they are not dramatic. Better and faster code is possible. In K_3 kernel shown above, each thread is responsible for computing a and b for all n . In this implementation we do not use shared memory buffer at all. Here instruction level parallelism within loop provides very big speed improvement comparing to kernels K_1 and K_2 . We can unroll loop to gain a bit more speed. In kernel K_4 loops are unrolled twice and in K_5 four times. We can also notice by looking at Fig. 4 that steps n and $n+2$ share a and b values at $n+1$. We take advantage of this in kernel K_5 , where we split each loop into two, each stepping over n with step 2, i.e. one loop with $n=[0,2,4,\dots]$ and another one with $n=[1,3,5,\dots]$. In each loop we store a and b values at $n+1$ in registers and reuse them. This provides additional speed boost without any unrolling. Due to register pressure loop unrolling in K_6 does not provide any more speed gain and may even result in program becoming slower.

6. Results

We compare time needed to perform complete time evolution of f between all of the above mentioned implementations, CPU and 6 CUDA implementations. Also OpenMP³ version of CPU implementation was tested. All code used `float` data type for storing $a_{n,m}$ and $b_{n,m}$. We found that using `double` data type did not affect precision nor correspondence of results with known solutions. On the other hand GTX680, being consumer grade GPU, lacks in capability of performing calculations on `double` and its performance degrades noticeably when switching from `float` to `double`. Strait CPU implementation was single threaded and was tested on "Intel Core i7-3770" running at 3.4GHz. CUDA implementations were tested on NVidia GTX680 with 2GB or RAM. Results of each test case are presented in Table 1. Test cases involved running each program 10 times and averaging resulted total run time. Actual run times are not important for they

³OpenMP - Open Multi-Processing, implementation of multithreading

| Impl: | CPU | OpenMP | K_1 | K_2 | K_3 | K_4 | K_5 | K_6 |
|-----------------|------|--------|-------|-------|-------|-------|-------|-------|
| Run Time (sec): | 5216 | 1537 | 87.1 | 85.3 | 46.8 | 45.3 | 45.5 | 43.85 |
| Speed Up Times: | 1 | 3.4 | 60 | 61 | 111 | 115 | 114 | 118 |
| MLUPS: | 9 | 31 | 551 | 562 | 1025 | 1059 | 1054 | 1094 |

Table 1: Results of testing of different implementations for a given set of parameters. CPU implementation is single threaded running on Intel i7-3770 3.4 GHz. OpenMP implementation run on the same CPU with 8 threads. The rest are CUDA versions run on GTX680. K_1 - one thread per lattice point. K_2 - same as K_1 , but using shared memory. In kernel K_3 and The rest of kernels each thread computes next values for all lattice points with a given m -number, as seen in Fig. 4. In K_4 main loops are unrolled twice and K_5 four times. In K_6 each loop over m is split in two, each stepping over 2 elements with lattice values reused in registers.

depend on passed parameters. Run time speed was compared against CPU implementation baseline and is presented as X times speed up. All CUDA implementations were tuned by varying block and grid sizes. It is common to measure lattice algorithms performance in Million Lattice Updates Per Second (MLUPS). That parameter is also shown. Note that in calculation of MLUPS we count update on movement only from time t to $t + 1$, i.e. on the whole grid only. Otherwise, if we include updates on the fractional grid, values of MLUPS would have to be doubled. Attained peak performance is 1094 MLUPS. Faster memory bandwidth and greater number of ALUs in later GPUs such as GTX-Titan (memory bandwidth 288GB/sec; 2688 CUDA cores) should give significantly higher peak value of MLUPS. For comparison, GTX680 used for this work has memory bandwidth of 192 GB/sec and 1536 CUDA cores (ALUs). On the example of our Boltzmann solver code you can see that even a consumer grade video card provides significant speed boost to computational tasks amenable to parallelisation. And if we take in the account low cost of such video cards, it is now possible to perform computations on the scale which just few years ago would require access to expensive supercomputers.

7. Conclusion

In this work we formulated numerical algorithm for solving Boltzmann transport equation applicable to semiconductor superlattice. Several different implementations of the algorithm were presented. One written in C for CPU and several for NVidia GPU using CUDA. We show that even in the most "naive" conversion of C to CUDA 16 fold speed performance is attained. Trying different optimization techniques discussed in this work CUDA code attains 118 fold speed improvement over the single threaded C code.

8. Acknowledgement

Author expressed gratitude to Kirill Alexseev and Jukka Isohäätälä for very useful discussions while working on this paper.

References

- [1] L. Pareschi, G. Russo, An introduction to monte carlo method for the boltzmann equation, ESAIM: Proceedings 35 (10).
- [2] D. Raabe, Overview of the lattice boltzmann method for nano- and microscale fluid dynamics in materials science and engineering, Modelling and Simulation in Materials Science and Engineering 12 (6) (2004) R13.
URL <http://stacks.iop.org/0965-0393/12/i=6/a=R01>
- [3] J. Tlke, Implementation of a lattice boltzmann kernel using the compute unified device architecture developed by nvidia, Computing and Visualization in Science 13 (1) (2010) 29–39. doi:10.1007/s00791-008-0120-2.
URL <http://dx.doi.org/10.1007/s00791-008-0120-2>
- [4] M. Mawson, A. Revell, Memory transfer optimization for a lattice boltzmann solver on kepler architecture nvidia gpus, CoRR abs/1309.1983.
- [5] M. Januszewski, M. Kostur, Sailfish: a flexible multi-GPU implementation of the lattice Boltzmann method, ArXiv e-prints arXiv:1311.2404.

- [6] Y. Kloss, P. Shuvalov, F. Tcheremissine, Solving boltzmann equation on {GPU}, *Procedia Computer Science* 1 (1) (2010) 1083 – 1091, [jce:title_iICCS 2010_i/ce:title_j. doi:http://dx.doi.org/10.1016/j.procs.2010.04.120](http://dx.doi.org/10.1016/j.procs.2010.04.120).
URL <http://www.sciencedirect.com/science/article/pii/S1877050910001213>
- [7] A. Frezzotti, G. P. Ghiroldi, L. Gibelli, Solving the Boltzmann equation on GPUs, *Computer Physics Communications* 182 (2011) 2445–2453. arXiv:1005.5405, doi:10.1016/j.cpc.2011.07.002.
- [8] A.-T. Pham, C. Jungemann, B. Meinerzhagen, On the numerical aspects of deterministic multisubband device simulations for strained double gate pmosfets, *Journal of Computational Electronics* 8 (3-4) (2009) 242–266. doi:10.1007/s10825-009-0301-3.
URL <http://dx.doi.org/10.1007/s10825-009-0301-3>
- [9] M. Ivaro, M. Carretero, L. Bonilla, Numerical method for hydrodynamic modulation equations describing bloch oscillations in semiconductor superlattices, *Journal of Computational Physics* 231 (13) (2012) 4499 – 4514. doi:http://dx.doi.org/10.1016/j.jcp.2012.02.024.
URL <http://www.sciencedirect.com/science/article/pii/S0021999112001337>
- [10] T. Hyart, J. Mattas, K. N. Alekseev, Model of the influence of an external magnetic field on the gain of terahertz radiation from semiconductor superlattices, *Phys. Rev. Lett.* 103 (2009) 117401. doi:10.1103/PhysRevLett.103.117401.
URL <http://link.aps.org/doi/10.1103/PhysRevLett.103.117401>
- [11] A. Wacker, Semiconductor superlattices: A model system for nonlinear transport, *Phys. Rep.* 357 (2002) 1.
- [12] L. Esaki, R. Tsu, Superlattice and negative differential conductivity in semiconductors, *IBM J. Res. Dev.* 14 (1970) 61–&.
- [13] J. Crank, P. Nicolson, A practical method for numerical evaluation of solutions of partial differential equations of the heat-conduction type, *Advances in Computational Mathematics* 6 (1) (1996) 207–226. doi:10.1007/BF02127704.
URL <http://dx.doi.org/10.1007/BF02127704>
- [14] E. Forest, Geometric integration for particle accelerators, *Journal of Physics A: Mathematical and General* 39 (19) (2006) 5321.
URL <http://stacks.iop.org/0305-4470/39/i=19/a=S03>
- [15] H. Yoshida, Recent progress in the theory and application of symplectic integrators, *Celestial Mechanics and Dynamical Astronomy* 56 (1-2) (1993) 27–43. doi:10.1007/BF00699717.
URL <http://dx.doi.org/10.1007/BF00699717>
- [16] S. Ryoo, C. I. Rodrigues, S. S. Baghsorkhi, S. S. Stone, D. B. Kirk, W.-m. W. Hwu, Optimization principles and application performance evaluation of a multithreaded gpu using cuda, in: *Proceedings of the 13th ACM SIGPLAN Symposium on Principles and Practice of Parallel Programming, PPOPP '08*, ACM, New York, NY, USA, 2008, pp. 73–82. doi:10.1145/1345206.1345220.
URL <http://doi.acm.org/10.1145/1345206.1345220>
- [17] S. Ryoo, C. I. Rodrigues, S. S. Baghsorkhi, S. S. Stone, D. B. Kirk, W.-m. W. Hwu, Optimization principles and application performance evaluation of a multithreaded gpu using cuda, in: *Proceedings of the 13th ACM SIGPLAN Symposium on Principles and practice of parallel programming*, ACM, 2008, pp. 73–82.
- [18] NVidia, Nvidias next generation cuda compute architecture: Kepler gk110 (2012).
URL <http://www.nvidia.com/content/PDF/kepler/NVIDIA-Kepler-GK110-Architecture-Whitepaper.pdf>
- [19] NVidia, *Cuda c programming guide* (2013).
URL <http://docs.nvidia.com/cuda/cuda-c-programming-guide>
- [20] J. Sanders, E. Kandrot, *CUDA by Example: An Introduction to General-Purpose GPU Programming*, 1st Edition, Addison-Wesley Professional, 2010.
- [21] N. Wilt, *The CUDA Handbook: A Comprehensive Guide to GPU Programming*, Pearson Education, 2013.